IEEE Access
Multidisciplinary | Rapid Review | Open Access Journal

Date of publication xxxx 00, 0000, date of current version xxxx 00, 0000.

Digital Object Identifier 10.1109/ACCESS.2017.DOI

Laser diode PWM control and its consequences on optical characteristics

MIROSLAV SLOUKA[1,2], LUKAS FOLTA [3], LADISLAV STANKE[4], JAN LATAL[1] (Member, IEEE) and PETR SISKA[1]

[1]Department of Telecommunications, Faculty of Electrical Engineering and Computer Science, VSB–Technical University of Ostrava, Ostrava, (e-mail: miroslav.slouka.st@vsb.cz)
[2]Development Lighting Technology, Photometry and Light Metrology, HELLA AUTOTECHNIK NOVA, Mohelnice, Czech Republic
[3]Department of Microelectronics, Faculty of Electrical Engineering and Communication, Brno University of Technology, Brno, Czech Republic
[4]Department of Psychology, Faculty of Arts, Palacky University Olomouc, Olomouc, Czech Republic

Corresponding author: Miroslav Slouka (e-mail: miroslav.slouka.st@vsb.cz).

This work was supported by project SP2022/18 and this research was also supported by the European Regional Development Fund—Operational Programme research, Development and Education, grant number CZ.02.1.01/ 0.0/0.0/17_049/0008425 (Research Platform focused on Industry 4.0 and Robotics in Ostrava agglomeration).

[

ABSTRACT This article deals with frequency PWM (pulse-width modulation) control methodology and experiments related to a deep characterization of InGaN (Indium gallium nitride) EELs (Edge Emitting Lasers) and the influence of drive current shape on power and spectral characteristics. The aim is to study wavelength tuning possibility and near-threshold region behavior that is usually not described in device datasheets. The publication consists of three main parts where different possible methods of output control are discussed. The CW (continuous wave) characteristics are displayed in the first part which describes the behavior of the LDUT (laser diode under test) in more detailed manner than in the available datasheets. The following part shows PWM control with a delayed rising edge of the drive current which enables frequency control. The third part ultimately shows the behavior using PWM with a rectangular drive current shape.

INDEX TERMS CW, drive current influence, EEL, laser, laser diode, laser diode control, PWM, spectrometry, radiometry, frequency control, laser diode metrology.

]

I. INTRODUCTION

VARIOUS scientific and industrial applications often demand an additional modification of the original laser output to meet the requirements for beam shape, diameter, peak fluence, and other beam parameters in order to perform the specific task or operation. For that purpose, laser light modulation is employed. Light modulation can be achieved with the use of different approaches. Laser light can be modulated internally via simple control of injection or driving current, or via more sophisticated approaches like intracavity modulators that are directly affecting laser resonator parameters [1]. Direct modulation of semiconductor lasers has been already studied in the past [2] as well as its limitations due to the chip parasitics [3]. Direct modulation of semiconductor lasers can be achieved by amplitude, pulse or frequency modulation [4]. US patent [5] describes an approach using a PWM current drive. With the application of temperature feedback and PWM current control, it is possible to achieve maximum optical output and efficiency. PWM driver modulation was also tested for an Erbium Doped Fiber Amplifier with a pump laser operating in such a mode [6]. There are major advantages to such a type of driving. The first is the heat dissipation reduction in the driver devices, leading to the possible use of small-sized heatsinks and reduction of the area occupied by the electronic circuit. There is, however, another advantage not related to energy consumption and heat dissipation. Such an approach is able to provide more stable optical power emission at very low levels, near the threshold region. Also, the relatively long relaxation time of erbium in the aforementioned study causes the laser emission occurs above a certain frequency, the output signal generated by the erbium-doped fiber does not vary significantly in power. Therefore, in such a case the PWM-based output signal is approximately the same as the one generated with the use of the regular CW mode. In the literature, it is possible to find both simulations [7] and also circuit designs [8] for PWM drivers designed to be used in conjunction with semiconductor lasers as well.

Nowadays, the PWM driving technique is mainly employed for the fine-tuning of LEDs' optical parameters for

example in the case of output PWM signal can be controlled by tuning the power of the analog input [9]. This is advantageous, especially for the RGB LEDs, to achieve demanded color precision [10], [11]. Conversely, PWM driving is also of interest due to its influence on LED lifetime [12]. In this case, the PWM current driving was tested up to 500 Hz. Another work [13] was focused on simulation and practical demonstration that the frequency deviation of the laser emission due to current (intensity) modulation alters the dynamic state and boundary conditions of the system such that even under large optical feedback strength, the laser may attain stability and retain a single modal state. Furthermore, applications of PWM in laser technology are widely used, especially to control output power in various industrial applications [14]–[20]. Laser diode (LD) PWM driving can be also advantageous for LD lighting applications. In such a case PWM driving enables speckle-free dimming as the PWM is more suitable to suppress speckle contrast than DC driving [21]. The potential to employ LDs is also rising in automotive, where the LDs can be implemented as a part of headlights. This is studied by Lin et al. [22] with the use of OSRAM PL TB405B LD. In this case, duty cycles were adjusted from 10 to 100%, as well as temperatures from -20 to 45 °C. The frequency was set to 400 Hz. In their latter paper, they [23] investigated the influence of three driving frequencies - 100, 250, and 400 Hz. Hence, it is of high interest to analyze how this relatively simple modulation approach can be employed to modulate the optical output of the commercially available semiconductor LDs also from the perspective of other relevant electrical and optical parameters modulated by PWM. And moreover, to make these results available for the whole scientific and engineering community, which might need these additional performance characteristics usually not contained within regular datasheets and are needed for specific LD applications in the field. For the experiments described in the presented paper two LDs made by OSRAM are chosen, specifically, **PLT5 520B** [24] and **PLT5 450B** [25]. Optical power and spectral parameters are compared for the case of CW and PWM input current drives in combination with the aforementioned LDs.

In the presented paper the influence of various PWM frequencies (10, 20, 30, 40, and 50 kHz, respectively) in combination with duty cycles between 0 and 100% is demonstrated and compared with the results acquired during the CW current driving of selected LDs.

II. LASER DIODES SPECIFICATIONS

Both of the chosen LDs OSRAM **PLT5 520B** [24] and **PLT5 450B** [25], respectively, used for the experiments described within this paper have an optical output power of 80 mW. Basic LDs parameters are contained within Tab. II-.1.

These LDs are low-cost, single-mode, edge-emitting lasers (EEL). Semiconductor chips of these LDs made of Indium Gallium Nitride heterostructures are mounted in the hermetically sealed metal case of TO56 type. This type is usually

TABLE II-.1. LD basic parameters [24] [25].

LD	PLT5 520B	PLT5 450B
max. current	240 mA	165 mA
peak wavelength	515 - 530 nm	440 - 460 nm
FWHM	1 nm	2 nm
operating temperature	-20 to +60 C°	-40 to +70 C°
threshold current	40 - 90 mA	17 - 60 mA

used for projection systems, spectroscopy, biomedical technologies, etc. The internal structure of the **PLT5 520B** (with cut-up cap) is shown in Fig. II-.1.

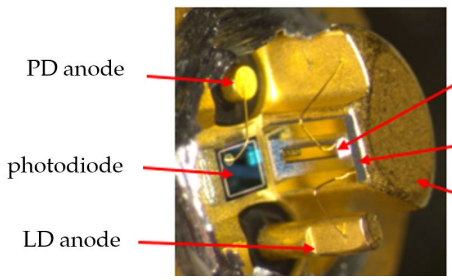

FIGURE II-.1. Internal structure of the **PLT5 520B** (with cut-up cap) magnified by the microscope.

III. EXPERIMENT I. - CONTINUOUS WAVE (CW)

A. CONTROL METHODS AND REALIZATION

The aim of the presented experiments is to measure the power characteristics of two selected LDs with the CW current driving. These characteristics are the dependence of optical power P_{opt} on the current through the LD I_{ld}, the dependence of central wavelength λ_p on the current, and the dependence of the threshold current I_{th} on the LD temperature ϑ. A spectrometer from Avantes, AvaSpec, is used for these tasks. The block diagram is shown in the picture III-A.1.

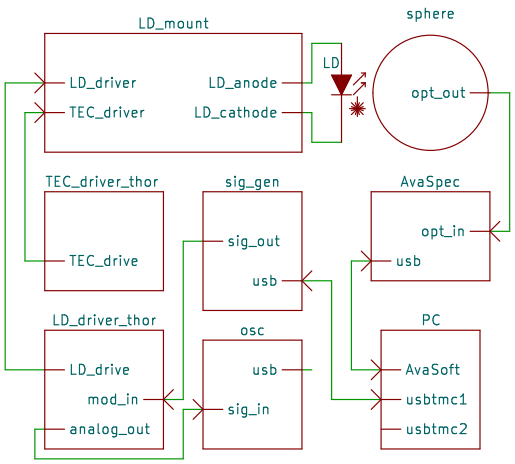

FIGURE III-A.1. Block diagram of the experiment with CW and slow PWM driving.

The used LD driver (TEC_driver_thor and LD_driver_thor) made by Thorlabs does not have an IEEE interface implemented for measurement automation. Hence, the temperature setting is manually operated. Nevertheless, the current setting can be modulated via BNC input "MOD IN", which is connected to the programmable voltage generator (sig_gen). Unfortunately, the set voltage value did not always correspond with the measured current on the LD driver meter. A correction curve is, therefore, measured. During the measurement itself, the set value of the voltage on the generator is noted and then recalculated using a correction curve to the value displayed by the LD driver ammeter. Thorlabs' LD driver also features an "ANALOG OUT" output, to which a voltage corresponding to the current LD current is applied. For measurements in CW mode, this port is connected to the oscilloscope only for indicative measurements and the oscilloscope data are not further used. LD and TEC drivers are connected to a dedicated mount made by Thorlabs (LD_mount), which enables temperature stabilization of the LD, and in which the LD itself is installed. The LD light beam is collected by a passive integrating sphere, which is connected by an optical cable to the spectrometer. The Avantes spectrometer is supplied in the basic package with a GUI only, therefore, without the possibility of programming and automation. This obstacle is resolved by using the programmable mouse and keyboard interface of xdotool. Thus, the AvaSoft GUI itself runs on a virtual PC with Windows 7, which is accessed by the xdotool program. Communication with the programmable measuring instruments (oscilloscope and generator) is provided using the usbtmc driver implemented in the Linux kernel itself.

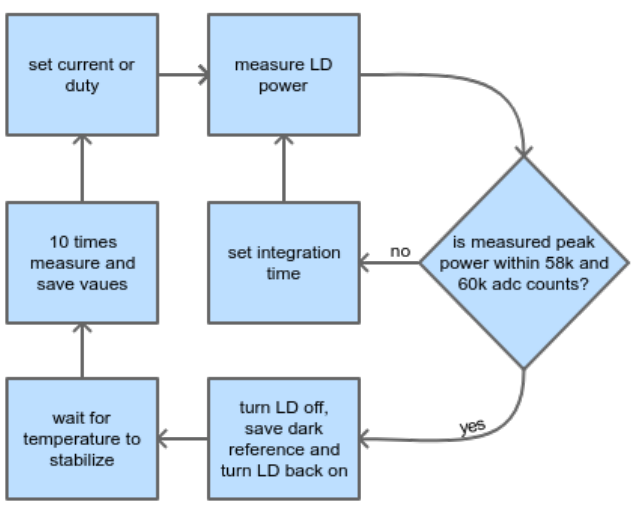

FIGURE III-A.2. Concise flow chart of the measuring algorithm for a single power characteristic.

A measurement program whose algorithm is outlined in the flowchart III-A.2, is running on the LXLE OS (Ubuntu derivative). This program is connected to the two usbtmc ports. In this OS the virtual system with the AvaSoft program is operated as well and with the use of shared storage, the spectral data are ultimately retrieved. The measurement program starts by setting the initial integrating time and storing the dark reference. It continues by setting the initial current, after which the peak value of the spectral curve is analyzed. If this value is not between 58k and 60k of the measured value of the employed 16-bit resolution ADC, then a new integrating time must be set and the test repeated until the spectrometer is calibrated to the optimum saturation level. After this test, the LD is briefly switched off to measure the dark reference. While the LD is switched back on to its previous state, the thermal stability of the LD is affected, so at this stage, it is necessary to wait for the LD temperature to stabilize again. The program determines the time of this delay based on the current passing through the LD. Lower current values lead to lower radiated LD power, which means less disturbance of thermal stability, and thus shorter delays. For currents above approx. 50 mA and duty cycles corresponding to these currents, the temperature stabilization took 3 minutes. After the described stabilization, 10 values of optical power and central wavelength are measured, which are averaged by Avasoft from 10 additional measured values. Upon recording the required values for a single current value, the entire cycle is repeated with the incremented current value. And then this process is repeated until the maximum current values are measured.

LDs used in this experiment are operated within a continuous wave (CW) regime - with a constant current value. The experimental system consisting of laboratory low-noise benchtop LD and temperature controller THORLABS ITC510 and cooled LD mount TCLDM9 [26] is employed. Benchtop LD controller's current can be set up to $1\ \mathrm{A} \pm 1\ \mathrm{mA}$ with a minimum step of $0,1\ \mathrm{mA}$.

The benchtop LD controller allows temperature control of the LD housing from $-45\ ^\circ\mathrm{C}$ up to the $+145 \pm 0,1\ ^\circ\mathrm{C}$. The LDs are attached by a contact surface to a copper plate heated by a TEC (thermoelectric cooler) employing the Peltier effect. Sample thermogram for the set value $\vartheta = 50 \pm 0,1^\circ\mathrm{C}$ of LD **PLT5 450B** mounted in this manner is depicted in Fig. III-A.3 (captured by thermal imaging camera FLIR T200 - ambient temperature in the laboratory $\approx 23\ ^\circ\mathrm{C}$). This figure proves the accuracy of the temperature stabilization of the TEC driver for all further experiments.

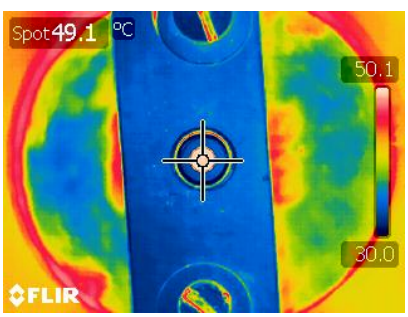

FIGURE III-A.3. Thermogram of non-emitting LD **PLT5 450B** at $\vartheta = 50\ \pm 0,1^\circ\mathrm{C}$.

B. RESULTS

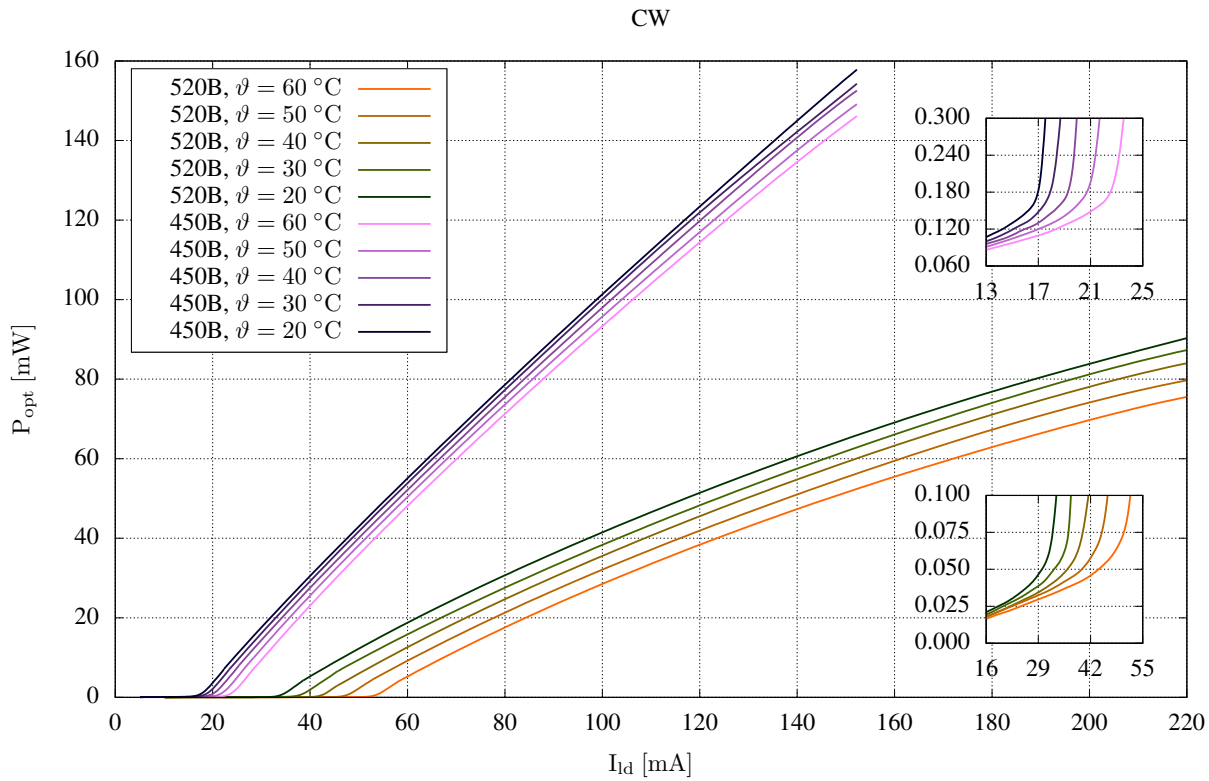

FIGURE III-B.1. Optical power characteristics of both LDUT at different operating temperatures in CW mode.

The first results obtained from the measurement are shown in the figures III-B.1 and III-B.2 show the behavior of LDUT in CW mode. Power and peak wavelength characteristics are measured from the range of temperatures 20 °C to 60 °C with 10 °C step.

The power characteristics in Figure III-B.1 confirm the datasheet data. It can be seen that for the LD 450B from the 24 mA value the power increases linearly, which is the area that is suitable for modulating the optical power. In contrast, the liner area for the LED 520B is not as uniform and, therefore, less suitable for modulating the optical power.

Threshold current is between **34 - 53 mA** and **16 - 24 mA** with max power between **75 - 90 mW** (220 mA) and **145 - 155 mW** (150 mA). As the temperature increases, the power decreases, and the threshold current increases. This dependence of threshold current on temperature is shown in Figure III-B.2 and confirmed by the increasing exponential character.

Figures in the annex (A-A.1 and A-A.2) show the Peak wavelength dependence on CW current. As in the case of the power measurements, also in the case of spectral parameters, the datasheet parameters were confirmed, i.e. the range below the threshold 531 - 521,5 nm and **456 - 449,5 nm**, above threshold 521,5 - 524 nm and **449,5 - 454 nm**. The theoretical assumption that the peak wavelength sharply increases with increasing current below the threshold and then not so significantly increases again with the current in the range above the lasing threshold is confirmed.

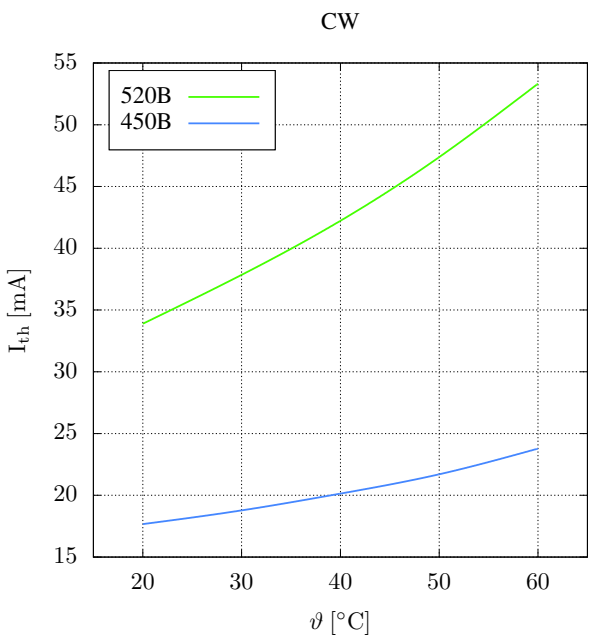

FIGURE III-B.2. Dependence of threshold current on the temperature of both LDUT in CW mode.

IV. EXPERIMENT II. - PULSE WIDTH MODULATION (PWM)

In initial experiments, several measurements were made with PWM slow, describing the rationalization of modulation using a commercial driver with a "slow" leading edge. Results obtained from measurements of the selected LD types' behavior at set frequencies and relative optical output power are presented, including distortion calculations.

A. CONTROL METHODS AND REALIZATION

1) Theoretical expression of power characteristics

Modulation of the LD current waveform by pulse width modulation (PWM), is used to achieve, among other things, the desired mean optical power of the laser beam. Consider the ideal case where the shape of the current waveform is perfectly rectangular. Or when the rising edge time - the duration for which the current rises from zero to its maximum - is zero. And this would also be true for the falling edge. In that case, the mean current of one period and their integer increments can be expressed

$$I_s = I_{max} \cdot (w_{ld}/100)\ [\mathrm{A}] \tag{IV-A.1}$$

where I_s [A] is mean current, I_{max} [A] is maximum current and w_{ld} [%] is duty cycle. At a 10% duty cycle, the mean current is one-tenth of the maximum, at 50% half, etc. If the dependence of the mean current on the duty cycle is plotted, it can be seen that the resulting waveform is purely linear, starting at zero and peaking at the value of the maximum current. And the same formula would apply to the dependence of optical power on the duty cycle

$$P_s = P_{max} \cdot (w_{ld}/100)\ [\mathrm{W}]. \tag{IV-A.2}$$

In the real-world situation, however, a rectangular current waveform is not achievable. The rising and falling edge times are always non-zero. Nevertheless, an integral part of PWM control is the modulation frequency, which allows the achievement of a nearly rectangular waveform even when the edge duration is non-zero. The condition for this is that the modulation period

$$t_{pwm} = 1/f_{pwm}\ [s] \tag{IV-A.3}$$

is significantly higher than the edge period t_{edg}. Simultaneously, it is assumed that the rising edge period is the same as the falling edge period: $t_{rise} = t_{fall} = t_{edg}$.

$$P_s(w_{ld}) \approx P_{max} \cdot (w_{ld}/100)\ [W],\ for\ t_{pwm} >>> t_{edg} \tag{IV-A.4}$$

Taking into account the duration of the duty cycle

$$t_{w_{ld}} = w_{ld}/(f_{pwm} \cdot 100)\ [\mathrm{s}] \tag{IV-A.5}$$

which depends on the PWM frequency, the dependence of the mean power on the duty cycle can be described even more accurately. If the duty cycle duration is shorter than the edge time, then the optical power will not reach its maximum. Under such conditions, the mean power will be less than in the ideal case. Similarly, if the duration of the duty cycle is longer than the period duration without the edge duration, then the optical power will not reach its minimum. Under such conditions, the mean power will be higher than in the ideal case. However, to express this behavior mathematically, several conditions need to be considered.

- First, the duration of the rising edge is equal to the duration of the falling edge $t_{rise} = t_{fall} = t_{edg}$. The real case will be rather close to this simplification. This is because the leading edge duration is caused by the same capacitance as the falling edge duration.
- Second, the waveform edges can be considered to be linear. In the reality, this will not be the case. However, a linear waveform is a good compromise between realistic behavior and the complexity of the approximating formula.
- Third, the nonlinearities in the LD power characteristic are not taken into account. That is, the relative optical power waveform is considered to have the same shape as the LD current waveform. This simplification is appropriate since their difference is not significant. $I_s(w_{ld}) \approx P_s(w_{ld})$

In such a case, the real dependence of the optical power on the duty cycle can be expressed using the following function.

$$\begin{aligned} P_s(w_{ld}) &= t_{w_{ld}}^2 \cdot \frac{P_{max}}{t_{edg}},\ for\ \ t_{w_{ld}} \in \langle 0, t_{edg}) \\ &= t_{w_{ld}} \cdot P_{max}\ \ for\ \ t_{w_{ld}} \in \langle t_{edg}, t_{pwm} - t_{edg}\rangle \\ &= (t_{pwm} \cdot P_{max}) - \left((t_{pwm} - t_{w_{ld}})^2 \cdot \frac{P_{max}}{t_{edg}}\right)\ [\mathrm{W}], \\ &for\ \ t_{w_{ld}} \in (t_{pwm} - t_{edg}, t_{pwm}\rangle \end{aligned} \tag{IV-A.6}$$

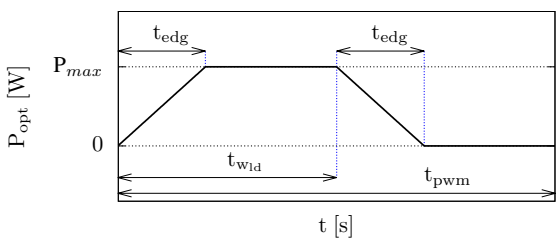

FIGURE IV-A.1. Plot illustrating variables used in the formula IV-A.6.

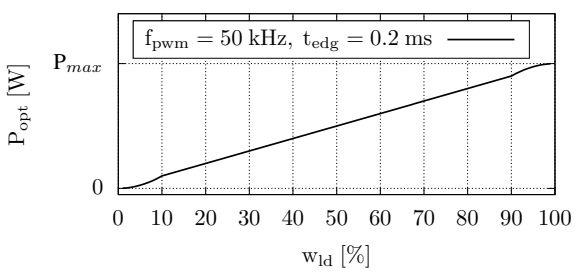

FIGURE IV-A.2. Example of theoretical power characteristic for a modulation frequency of 50 kHz and edge time of 0.2 ms.

2) Period measurement

The measurements of this experiment are carried out in almost the same configuration of measuring instruments as outlined in figure III-A.1. The only difference is that instead of the integrating sphere, the LD illuminates the active photodetector, which is connected directly to the oscilloscope. The control of the LD, i.e. the switching voltage, corresponds to the driving voltage during the measurement of spectral quantities.

The one-period pulse waveform for both LDs used are shown in Fig. IV-A.3 and IV-A.4. The maximum resolution of the oscilloscope is used, which is 2500 points on the horizontal scale and 2 bytes on the vertical scale, respectively. The periods of some frequencies fit exactly into the entire horizontal scale of the image, however, for some, it is necessary to export fewer horizontal points than 2500. This is due to the fact that the oscilloscope supports only a few specific horizontal scales presets.

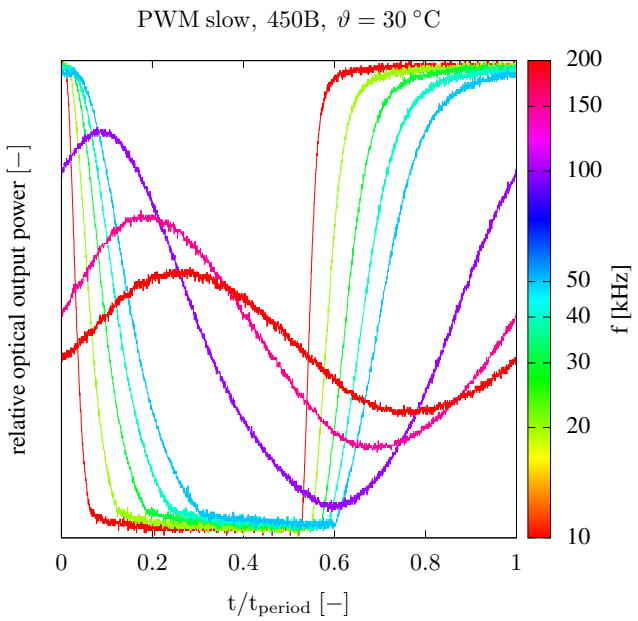

FIGURE IV-A.3. **PLT5 450B** relative optical power waveform per single signal period at different frequencies

3) Other measurements

This measurement is implemented in accordance with the block diagram III-A.1. The maximum LD current, that is, the active PWM level, is set using an oscilloscope to which the voltage from the "ANALOG OUT" port of the LD driver is applied. The current value represented by the voltage on this port is slightly different than the LD driver ammeter indicates. Therefore, for the correlation between the current on the LD driver ammeter and the voltage on the "ANALOG OUT" port, a correction curve is again measured to calculate a true current value, which is considered to be the one indicated on the LD meter. Exactly the same as in the CW mode case. The generated voltage is corrected to the valid

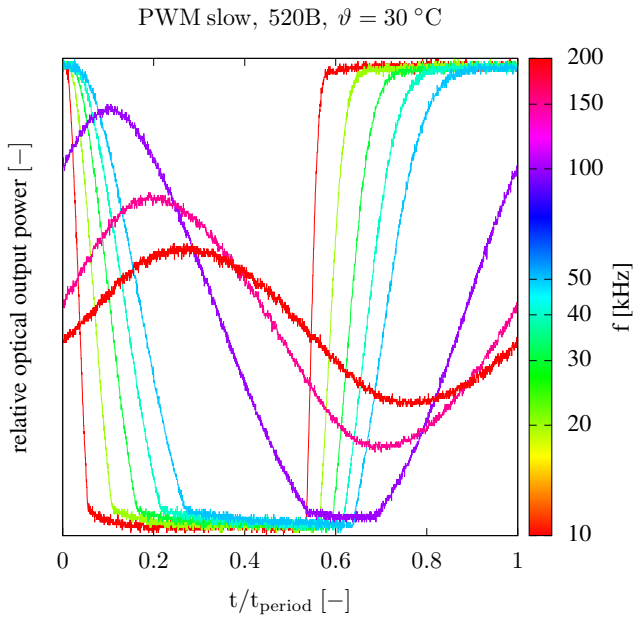

FIGURE IV-A.4. **PLT5 520B** relative optical power waveform per single signal period at different frequencies

current value displayed on the LD driver. From the maximum value of the current and the duty cycle, the mean value of the current passing through the LD can be calculated. However, the mean value of the current cannot be included in the graphs due to the imperfection of the pulse. For example, if the modulation frequency is high enough, that a non-zero transition time between zero and maximum LD current influences the power characteristic (due to the fact that the rising edge is not steep), then this characteristic will show that the LD does not start to emit until 10% of the duty cycle is reached, while before this threshold the LD does not emit at all and almost no current flows through the LD. The value of the current, which would be indicated in the graph e.g. at the point 8% of the duty cycle, would not correspond to reality. Meaning, that the traditional calculation of the mean current using the duty cycle and the maximum current is only valid for a current driving approaching an ideal square current waveform. The measurement algorithm is almost the same as in the CW mode. The difference is that only the duty cycle is set instead of the current itself.

Maximum current amplitudes for PWM LD drive selected with respect to recommended catalog values

- **PLT5 520B** - 220 mA,
- **PLT5 450B** - 150 mA.

Thus, the generator was set to a current corresponding to 220 mA and 150 mA respectively, after recalculation using the correction curve, the real values of the current in the active level were 216.1 mA and 148.1 mA.

B. PULSE DISTORTION DEPENDENCE ON FREQUENCY

From the data used to represent the current waveform in the graphs IV-A.3, IV-A.4, V-A.1 and V-A.2, representation of the signal distortion is calculated IV-B.1 V-A.3. For each current value "I_r" measured at a specific frequency and at a certain point of the period, a specific measure is calculated. This measure expresses the difference from the ideal current waveform "I_i" within the same point of the period, in relation to "p" peak-to-peak value of the ideal signal.

For each point of a given frequency, the deviation from the ideal waveform is calculated, and the average of these "n" points is calculated separately for each frequency. From the data used in the plots IV-A.3, IV-A.4, V-A.1 and V-A.2 showing the relative optical power waveforms during one PWM period, the optical output distortion waveforms as a function of PWM switching frequency were calculated using the IV-B.1 equation, see figures IV-B.1 and V-A.3.

$$\Delta = \frac{\sum \left[\frac{\sqrt{(P_{opt_r}(t) - P_{opt_i}(t))^2}}{P_{ref}} \cdot 100 \right]}{n} \, [\%] \qquad \text{(IV-B.1)}$$

Since in the real world, when PWM switching is employed, it is not possible to achieve an ideal waveform (orthogonal edges of pulses) of optical power over time, it is advantageous to have an approach to quantify this distortion. In this paper, the following method is applied. Each measured point of the optical waveform characteristic over time for a single frequency $P_{opt_r}(t)$ is compared to the value that an ideal $P_{opt_i}(t)$ waveform would have at that specific instance. From this difference, using a reference value P_{ref} corresponding to the value in the active level, the relative distortion for one measured point in time is calculated. Finally, the total waveform distortion for a single frequency is expressed as the arithmetic mean of all partial distortions over time of a single period. This approach is possible to apply due to the fact that the image data taken from the oscilloscope are synchronized with the input switching voltage.

Four values of P_{ref} are determined. This is for each combination of LD and PWM control circuits and it is necessary since when changing the LD or PWM control method, the position of the photodetector and LD needs to be optimally set again. And since the photodetector is very sensitive to this adjustment, each such change requires a new value for the reference relative optical power in the active and passive levels.

The reference points are determined as follows. One frequency with the least distorted waveform is selected. From this, a few points are selected at the end of the passive and active levels. Their arithmetic average subsequently determined the reference value in the active $P_{ref_{akt}}$ or passive part of the switching $P_{ref_{pas}}$. And the absolute value of their difference finally determined the bias reference

$$P_{ref} = |P_{ref_{akt}} - P_{ref_{pas}}|. \qquad \text{(IV-B.2)}$$

The function $P_{opt_i}(t)$ has an ideal PWM waveform with a 50% duty cycle, a frequency corresponding to the real waveform being compared, a passive level of $P_{ref_{pass}}$ and an active level of $P_{ref_{act}}$.

In the graph IV-B.1 a linear increase in a distortion from 10% to about 70% can be observed for both LDs. Starting from the maximum distortion recorded around the PWM frequency of 120 kHz, the distortion decreases with increasing frequency. The observed distortion trend is due to two effects. First, the phase shift of the LD optical output from the switching voltage (the trigger of the measured data is set to the input switching voltage). This results in the active level of the LD optical output being partially within the passive level of the input voltage, which results in a higher difference between the ideal and measured signal. This difference disappears at higher PWM frequencies as the second effect becomes more dominant. That is the gradual convergence of the output signal, up to a steady mean value. This is caused by switching so fast that the optical output fluctuates only on the pulse edges and does not reach its maximum and minimum in the active and passive levels. Thus, this way of interpreting distortion is affected by both the change in phase of the signal and the variation in its shape. The optical output of LD when switched with PWM will always converge to a steady state level with increasing frequency. E.g. if the PWM duty cycle is 50%, and at the same time both edges of the pulses are identical, then the steady-state level will be at 50% of the active level optical output. In this case, the distortion plot should converge to 50%. Such a case can be observed when switching with a PWM slow. In the IV-A.3 and IV-A.4 plots, the optical output converges to the steady-state level at the halfway point of the active level.

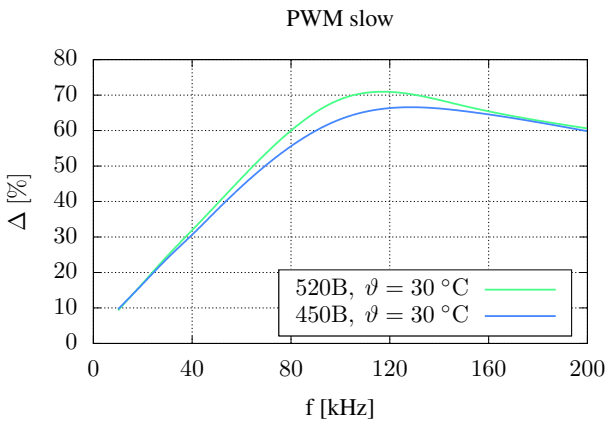

FIGURE IV-B.1. Distortion waveform of the real LD optical output compared to the ideal PWM waveform at 50% duty cycle as a function of PWM frequency.

C. RESULTS

Figures IV-C.1 and IV-C.2 show the dependence of power on pulse width in PWM slow mode. Both figures consist of five characteristics with frequency PWM from 10 kHz to 50 kHz with (10 kHz step) and one additional characteristic with frequency 50 kHz and temperature 60 °C. The slowed leading edge of the signal here causes a change in the threshold and therefore allows frequency control of the LDUT output.

Frequency control of the LDUT threshold is successful only in the range of 10 kHz to 50 kHz, where the diodes could be controlled so that the characteristics still have a linear waveform. Leading edge distortions at frequencies above 50 kHz cause nonlinearities of the waveform and frequencies below 10 kHz are not considered in the presented experiment. The maximum power in 30 °C corresponds to approx. **86 mW** and **147 mW** which is equal to CW mode. For 60 °C **74 mW** and **101 mW** are obtained, respectively.

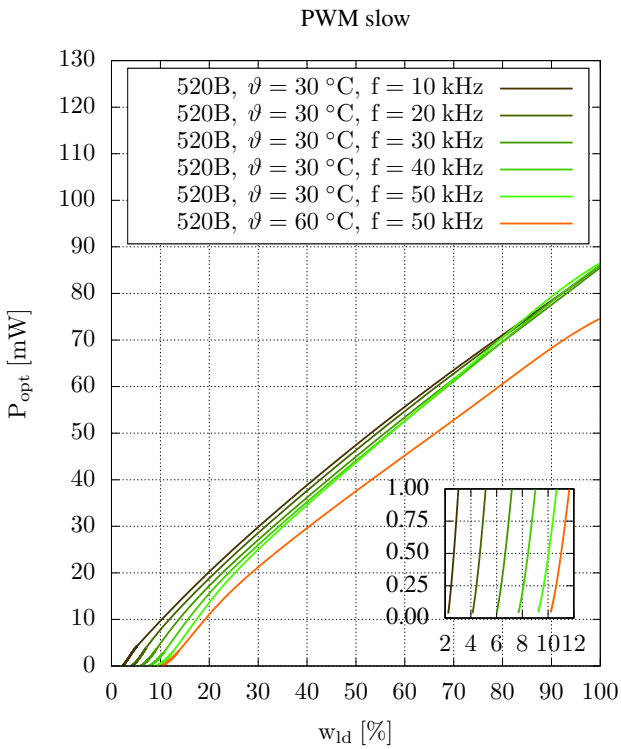

FIGURE IV-C.1. **PLT5 520B** optical power characteristics in PWM slow mode.

The dependence of thresholds in PWM slow control on frequency is shown in the figure. IV-C.3. In the aforementioned range of 10 kHz to 50 kHz, it is possible to control the threshold in the range of **2.5 - 9.9%** PWM (I_{ld} = 216.1 mA) and **2 - 6.7%** PWM (I_{ld} = 148.1 mA). The increased temperature causes the threshold to rise. This phenomenon increases with increasing frequency and, therefore, with distortion of the control signal. Peak wavelength characteristics are shown in the annex (Figure A-B.1 and A-B.2).

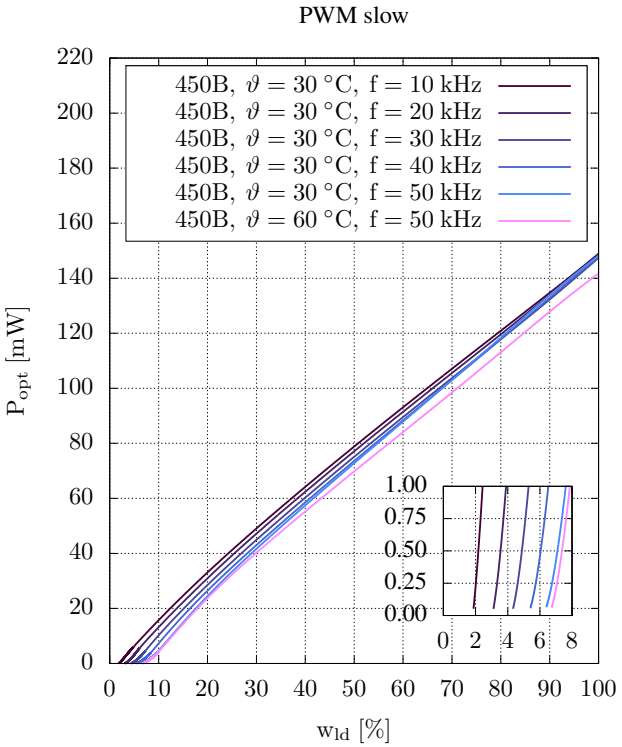

FIGURE IV-C.2. **PLT5 450B** optical power characteristics in PWM slow mode.

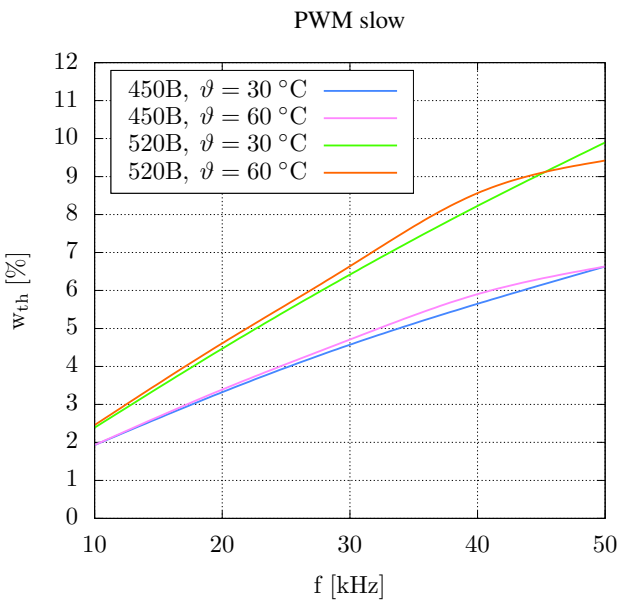

FIGURE IV-C.3. Dependence of threshold on the frequency of both LDUT in PWM slow.

V. EXPERIMENT III. - PULSE WIDTH MODULATION (PWM) USING EXTERNAL CIRCUITS

In the next section of this paper measurements with **PWM fast** are performed. It describes the implementation of modulation using a proprietary external electronic driver with a "fast" leading edge. Within this section, information regarding the circuit design of the driver is presented and the results are compared with the measurements performed in the previous chapter for PWM **slow**.

A. CONTROL METHODS AND REALIZATION

1) Period measurement

This experiment is carried out in almost the same configuration of measurement instruments as indicated in Fig. V-A.4. The difference is that instead of the integrating sphere, the LD illuminates the active photodetector, which is connected directly to the oscilloscope. The control of the LD i.e. switching and supply voltages corresponds to the control during the measurement of spectral quantities. The results of period measurements in PWM fast mode can be seen in the graphs V-A.1 and V-A.2. The distortion plot calculated from these data is shown in figure V-A.3. As a result, the switching times became significantly faster than in the previous (slow) driver case. Since the bandwidth was no longer limited to only about 50kHz, the results show a better correlation between the control signal and the output power. Output signal distortion is now under the 10% for all tested frequencies. [see Fig. V-A.3.]. The distortion here is primarily caused by the too-short duration of the rising and falling edges. In this case, oscillations are created at the beginning and end of the pulse, which is more noticeable with increasing frequency. (Fig V-A.4 and 5).

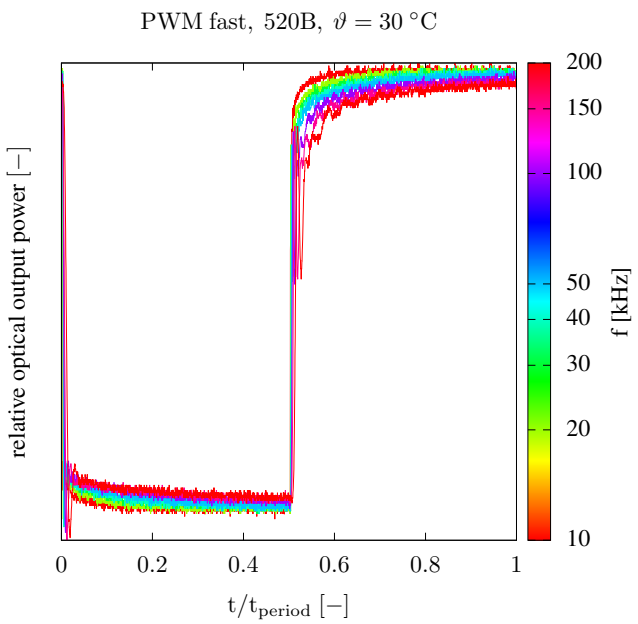

FIGURE V-A.1. **PLT5 520B** relative optical power waveform per single signal period at different frequencies in PWM fast mode

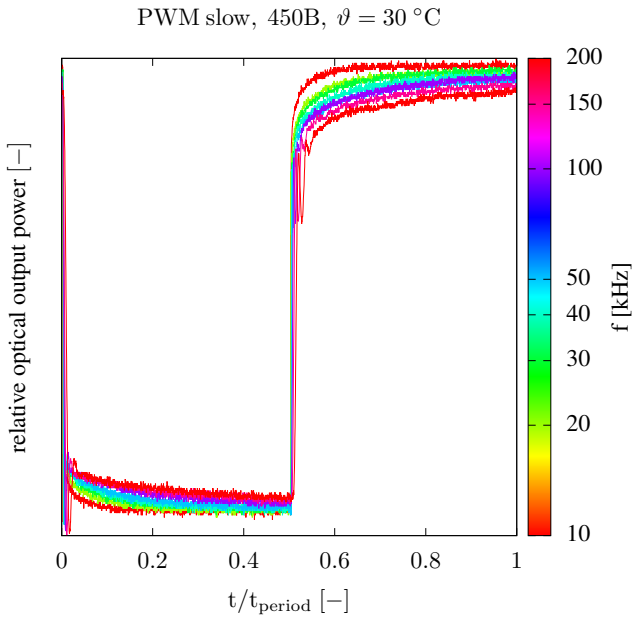

FIGURE V-A.2. **PLT5 450B** relative optical power waveform per single signal period at different frequencies in PWM fast mode

With fast PWM switching, see V-A.3, the distortion waveforms are highly non-linear. This is caused firstly by the oscillations of the LD optical output at the rise and fall of the pulse edge, secondly by the gradual decrease of the optical power in the active level with increasing frequency, and finally by the small frequency range of the measurement. These factors can be observed in the plots of V-A.1 and V-A.2. The maximum measuring frequency is too low to determine to what steady-state level the signal will converge. However, it can be said with confidence that the LD optical power waveform during a single PWM period is significantly less distorted for switching with PWM fast than it is with PWM slow.

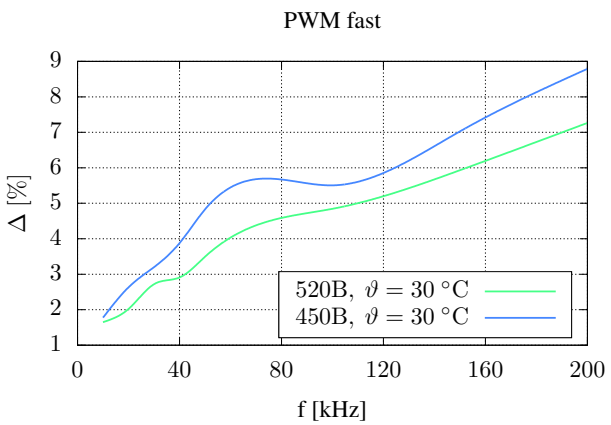

FIGURE V-A.3. Distortion waveform of the real LD optical output compared to the ideal PWM waveform at 50% duty cycle as a function of PWM frequency.

2) Other measurements

This measurement is implemented in accordance with the block diagram V-A.4.

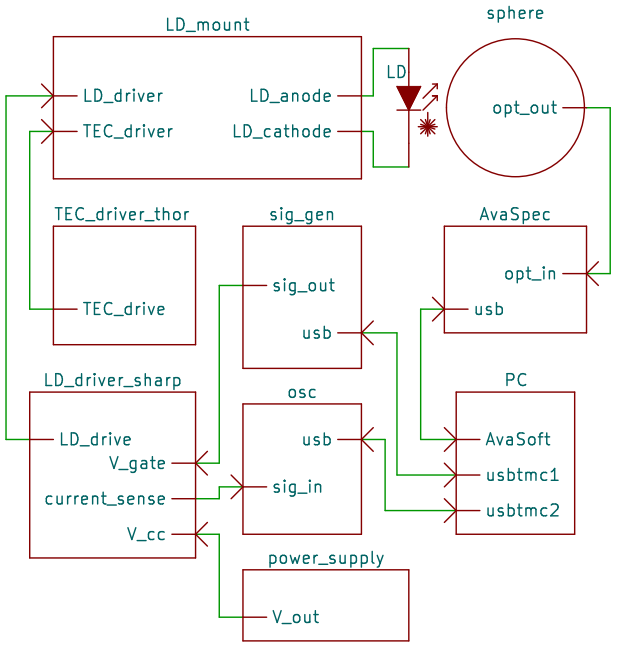

FIGURE V-A.4. Block diagram of the fast PWM driving experiment.

The maximum LD current, i.e. the active PWM level, is set using an oscilloscope to which the voltage from the "current sense" port of the LD driver is applied. This value is then also converted to a true value using a correction curve - the value is the one that would be displayed on the LD driver meter by Thorlabs. This setting is accomplished using the output voltage of the power supply, with full saturation of the switching transistors. Setting the maximum LD current using the switching gate voltage is not used due to temperature stability. The design of the driver is shown in Figure V-A.5.

Its main goal is to keep its structure as simple as possible. This is in order to achieve fast edges in LD switching. Possible current sources and other elements of a proper LD driver could deteriorate this parameter.

The circuit includes a mechanical switch for switching on and also LED to indicate that the circuit is turned on. Furthermore, coupling capacitors C1 and C2 with a total capacitance of 200 μF are employed. Resistor R2 is there for the stability of the set current and serves as a current source for the LD. Capacitor C3 is implemented to compensate for the induction on the wire to the LD, which stabilizes the current sweeps during switching. BS170 N-channel DMOSFET in the TO92 package is chosen as the switching transistor because of its good dynamic characteristics for current switching. To optimize the power load, two transistors are connected in parallel. On their gate is resistor R4 for base grounding, which is very desirable in unipolar transistors. And also R3 for additional gate protection. Resistor R5 is used to measure

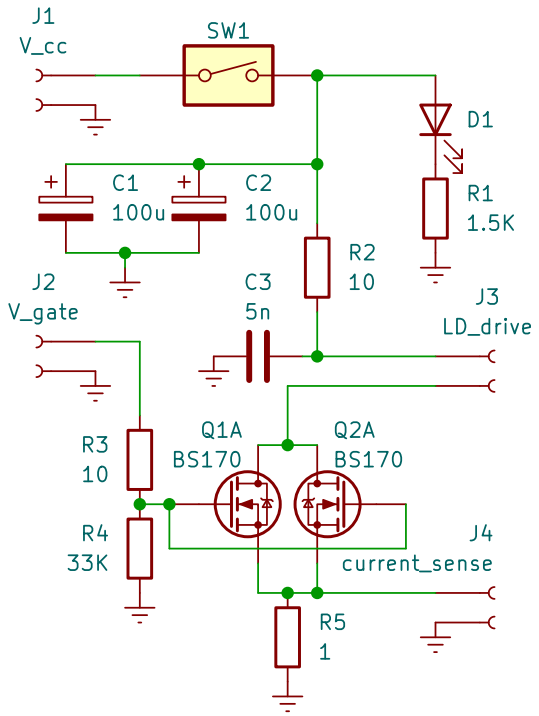

FIGURE V-A.5. Circuit diagram of the fast PWM control driver.

the current through the LD. The circuit was implemented using THT.

The measurement algorithm is almost identical to the CW mode. The difference is that instead of a current only the duty cycle is being set.

B. RESULTS

The optical power characteristics in PWM fast mode are shown in the figures V-B.1 and V-B.2, they are presented in the same manner as in the PWM slow case, i.e. five curves from the 10 to 50 kHz in steps of 10 kHz and an additional curve at 50 kHz at 60 °C. Also, the maximum power is consistent with previous measurements. It can be seen from the characteristics that with a nearly rectangular drive signal, there is no dramatic shift in the threshold when the frequency is changed in comparison to the PWM slow control. The change in threshold is only observed in the range **0.06 - 0.195%** and **0.05 - 0.195%**. Another difference in this type of control is the effect of temperature on the threshold change. In this case, it is only minimal and in the range under 0,02% for both LDUTs, as shown in Figure V-B.3. The waveforms of the peak wavelength characteristics are shown in the appendix as (figures A-C.1 and A-C.2).

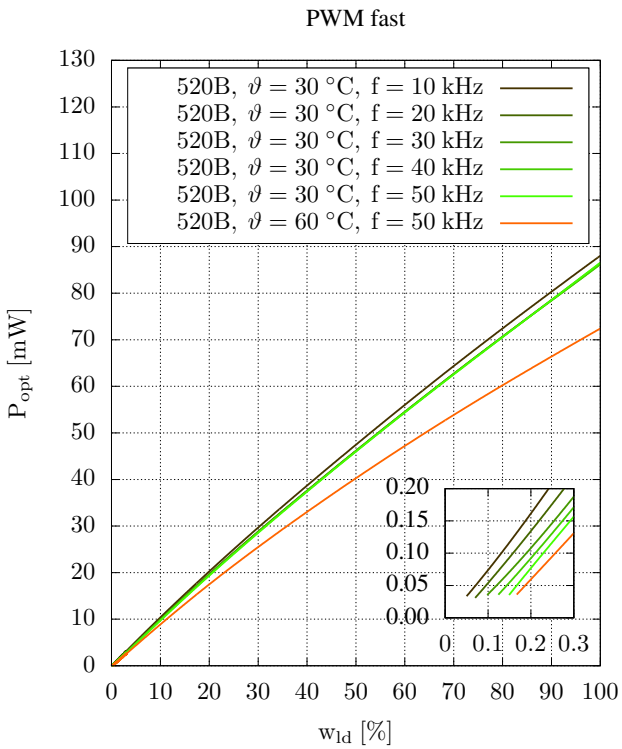

FIGURE V-B.1. **PLT5 520B** optical power characteristics in PWM fast mode.

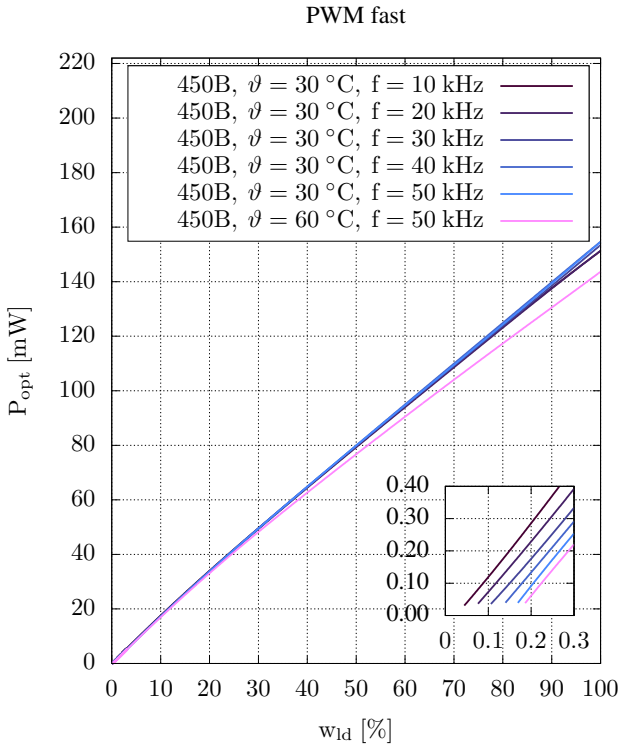

FIGURE V-B.2. **PLT5 450B** optical power characteristics in PWM fast mode.

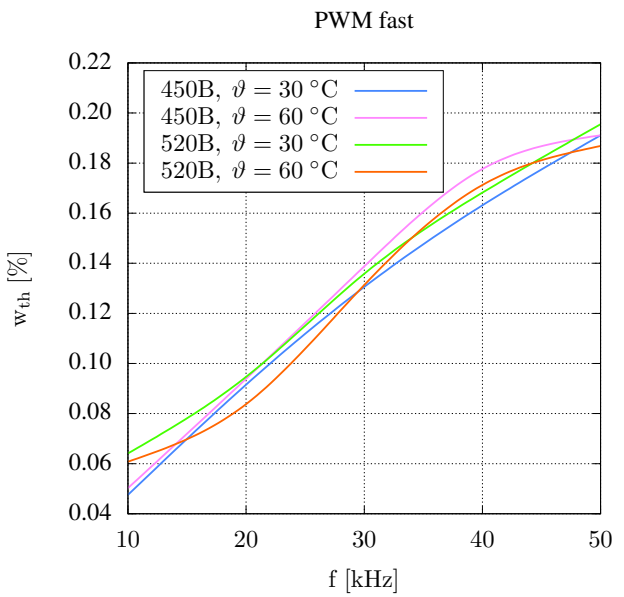

FIGURE V-B.3. Dependence of threshold on the frequency of both LDUT in PWM fast

VI. ICT510 CORRECTION CURVE

LD current measurements are performed in a different manner for each experiment. However, all the recalculated data are related by a correction curve to the value of current that the ICT 510 LD driver would show on its display.

- In CW mode, the LD current is set using the generator voltage applied to the "MOD IN" LD driver input. This voltage is recorded via USB port and recalculated using a correction curve to the current indicated by the LD driver.
- In PWM mode with slow edges, the current in the active

PWM level is set before the measurement started. The steady-state voltage from the generator is applied to the "MOD IN" input of the LD driver, and set to a value such that the oscilloscope measures a voltage corresponding to the required maximum current (150 mA or 220 mA) at the

"ANALOG OUT" output of the LD driver. Next, the required current is recalculated using a correction curve to the value that would be displayed by the LD driver.
- In PWM mode with fast edges, the current in the active PWM level is also set before starting the measurement. The voltage at the switch gate is set to provide full saturation of the conductive channel. The switch supply voltage is then set to a value such that the oscilloscope would measure a voltage corresponding to the required maximum current (150 mA or 220 mA) at the "CURRENT SENSE" LD switch output. Next, the required current was recalculated using a correction curve to the value that would be displayed by the LD driver.
The voltage to the current ratio for both ports of the LD driver is 10:1 $D_{io} = 10\ \mathrm{VA}^{-1}$.

TABLE VI-.1. Correction curves. Measured values of current displayed on LD driver I_{dr}, generator voltage on LD driver "MOD IN" U_{gen}, and voltage from LD driver"ANALOG OUT" U_{osc}. And relative current correction for generator K_{gen} and oscilloscope K_{osc}.

I_{dr} $[mA]$	U_{gen} $[V]$	U_{osc} $[V]$	K_{gen} [%]	K_{osc} [%]
9,7	0,1	0,100	-3,093	-3,093
19,9	0,2	0,205	-0,503	-3,015
40,3	0,4	0,417	0,744	-3,474
60,7	0,6	0,622	1,153	-2,471
81,0	0,8	0,833	1,235	-2,840
101,4	1,0	1,040	1,381	-2,564
121,8	1,2	1,220	1,478	-0,164
142,2	1,4	1,440	1,547	-1,266
162,6	1,6	1,650	1,599	-1,476
183,0	1,8	1,850	1,639	-1,093
203,4	2,0	2,070	1,672	-1,770
224,1	2,2	2,280	1,830	-1,740
244,5	2,4	2,490	1,840	-1,840
254,7	2,5	2,590	1,845	-1,688

To calculate the real value of the LD current from the voltage value at "MOD IN" the following equation applies:

$$I_{dr} = \frac{U_{gen}}{D_{io}} + \left(\frac{U_{gen}}{D_{io}} \cdot \frac{K_{gen}(U_{gen})}{100}\right)\ [\mathrm{A}] \qquad \text{(VI-.1)}$$

To calculate the true LD current value from the voltage value at "MOD OUT" the following equation applies:

$$I_{dr} = \frac{U_{osc}}{D_{io}} + \left(\frac{U_{osc}}{D_{io}} \cdot \frac{K_{osc}(U_{osc})}{100}\right)\ [\mathrm{A}] \qquad \text{(VI-.2)}$$

VII. MEASUREMENT UNCERTAINTIES

There are two basic types of uncertainties. *Type A uncertainty,* u_A (hereafter TAU), which is determined experimentally by repeated measurements.
It is the sample standard deviation of the sample mean $s_{\overline{x}}$, where x is the repeatedly measured quantity, $\overline{x}$ is the arithmetic mean of the measured quantity, and n is the number of measurements.

$$u_A(x) = s_{\overline{x}} = \sqrt{\frac{1}{n \cdot (n-1)} \cdot \sum_{i=1}^{n} (x_i - \overline{x})^2} \qquad \text{(VII-.1)}$$

Type B uncertainty, u_B (hereafter TBU), which is defined by other means than repeated measurements and may be determined by the specification of the measuring instruments. In this case, the TBU is equal to:

$$u_B = \frac{u_{instr}}{\chi} \qquad \text{(VII-.2)}$$

Where u_{instr} is the value obtained from the data sheet and χ is the distribution coefficient of the random variable. The coefficient of the *normal distribution* $\chi = 2$ was used for all calculations. The total TBU is determined by the geometric sum of all TBU sources:

$$u_B = \sqrt{\sum_{Z=1}^{n} u_{BZ}^2} \qquad \text{(VII-.3)}$$

Subsequently, the *combined standard uncertainty,* u_C (henceforth CSU) is defined as the geometric sum of the TAU and TBU:

$$u_C = \sqrt{u_A^2 + u_B^2} \qquad \text{(VII-.4)}$$

The probability that the true value of the measured random variable lies within the interval given by the combined standard uncertainty u_C for a normal distribution is 68%.
And finally, the *Extended Uncertainty,* u_R with an extension coefficient k_r. For all calculations, $k_r = 2$ is used for the *normal distribution*, which means that the measured value is within the range given by u_R with 95% probability.

$$u_R = k_r \cdot u_C \qquad \text{(VII-.5)}$$

It implies that if the uncertainty is given only by the accuracy of a single instrument, then the *extended uncertainty* is equal:

$$u_R = 2 \cdot u_B = 2 \cdot \frac{u_{instr}}{2} = u_{instr} \qquad \text{(VII-.6)}$$

1) LD temperature uncertainty

LD temperature uncertainty is manifested in both the spectrometer and photodetector measurements. Only the TEC driver actually contributed to the LD temperature uncertainty. The accuracy of the AD590 temperature sensor used is $u_{tec} = \pm 0,1\ ^\circ\mathrm{C}$ [27]. The LD temperature uncertainty is $u_{R\_TEC} = \pm 0,1\ ^\circ\mathrm{C}$ according to the equation VII-.6.

2) Photodetector measurement horizontal uncertainty

Only TBUs are determined in the photodetector measurements, i.e. $u_C = u_B$. Two factors are playing a major role in this case: the uncertainty of the photodetector and the oscilloscope.
The horizontal uncertainty is only contributed by

the oscilloscope, which has a horizontal accuracy of $u_{osc\_hor} = \pm 50\ ppm = \pm 0,005\%$ [28]. This is related to the value of the time base used. Thus, the horizontal uncertainty is $u_{R\_f\_hor} = \pm 0,005\%$ according to the formula VII-.6

3) Photodetector measurement vertical uncertainty

Both the photodetector and the oscilloscope contribute to the vertical uncertainty. The vertical accuracy of the photodetector is $u_{f\_vert} = \pm 2\%$ [29], of which the TBU according to the formula VII-.2 $u_{B1\_f\_ver} = \pm 2/2 = \pm 1\%$. The vertical accuracy of the oscilloscope is $u_{osc\_vert} = \pm 3\%$ [28], of which TBU by formula VII-.2 $u_{B2\_f\_ver} = \pm 3/2 = \pm 1,5\%$. The total vertical TBU of the photodetector data is according to the formula VII-.3 $u_{B\_f\_ver} = \sqrt{1^2 + 1,5^2} = \pm 1,8\%$. Finally, $u_{R\_f\_vert} = 2 \cdot \pm 1,8 = \pm 3,6\%$.

4) LD current uncertainty

The LD current is recalculated according to the ICT 510 correction curve. With this correction, the relatively high inaccuracy of the ICT 510 ports is eliminated from the calculations. For the LD current, only TBU ($u_C = u_B$) is calculated. This varies according to the experimental setup and is divided into TBUs in CW mode $u_{B\_s\_i\_cw}$ and in PWM mode $u_{B\_s\_imax\_pwm}$. In CW mode, only the uncertainty of the LD driver current output $u_{driv\_i} = \pm 1$ mA [27] contributes to the current TBU. The uncertainty of the current in CW mode is $u_{R\_s\_i\_cw} = \pm 1$ mA according to the formula VII-.6. In PWM modes, both $u_{driv\_i} = \pm 1$ mA [27] and the oscilloscope uncertainty $u_{osc\_vert} = \pm 3\%$ [28] contribute to the LD current TBU in PWM mode. The LD current TBU in PWM mode $u_{B\_s\_i\_pwm}$ has to be expressed only for maximum currents. Separately for green LD PLT5 520B $u_{B\_s\_imax\_pwm\_gr}$ and for blue LD PLT5 450B $u_{B\_s\_imax\_pwm\_bl}$, respectively.

The maximum currents PLT5 520B and PLT5 450B are according to the formula VI-.2:

$$I_{max\_pwm\_gr} = \frac{2,2}{10} + \left(\frac{2,2}{10} \cdot \frac{-1,77}{100}\right) \doteq 216,1\ mA$$
$$I_{max\_pwm\_bl} = \frac{1,5}{10} + \left(\frac{1,5}{10} \cdot \frac{-1,266}{100}\right) \doteq 148,1\ mA \quad \text{(VII-.7)}$$

Then, according to the formulae VII-.2, VII-.3 and VII-.5:

$$u_{B\_s\_imax\_pwm\_gr} = \sqrt{\left[\frac{u_{driv\_ild}}{\chi}\right]^2 + \left[\frac{u_{osc\_vert}}{\chi}\right]^2} = \sqrt{\left[\frac{\pm 1m}{2}\right]^2 + \left[\frac{\frac{216,1m}{100} \cdot (\pm 3)}{2}\right]^2} \doteq \pm 3,2798\ mA$$
$$u_{R\_s\_imax\_pwm\_gr} = 2 \cdot (\pm 3,2798m) \doteq \pm 6,6\ mA$$
$$u_{B\_s\_imax\_pwm\_bl} = \sqrt{\left[\frac{\pm 1m}{2}\right]^2 + \left[\frac{\frac{148,1m}{100} \cdot (\pm 3)}{2}\right]^2} \doteq \pm 2,2771\ mA$$
$$u_{R\_s\_imax\_pwm\_bl} = 2 \cdot (\pm 2,2771m) \doteq \pm 4,6\ mA \quad \text{(VII-.8)}$$

5) Optical power spectrometer measurement uncertainty

For each iteration of the current, 100 measurements are made with the spectrometer. However, only 10 values are available from which is possible to calculate the TAU using the formula VII-.1. For each spectrometer measurement, the internal spectrometer function and the Avasoft program are employed to take multiple measurements and average the measurements. This function offers the possibility to set the number of measurements to be taken after pressing the start icon in the GUI. The user is then presented with the arithmetic average of the number of measurements that the user has specified. In all experiments in this paper, this number is set to 10.

As a result, the recalculated values of P_{opt} and CWL are computed from the ten values from the raw data measured by the script, from which the TAU is consequently computed, and each of them is the result of ten measurements averaged in the Avasoft interface.

The use of this feature has two main implications for the experiments conducted. Firstly, the time for accurate measurements is reduced. By this is meant that if 100 measurements are averaged using only the measurement script, then the measurement time would increase dramatically due to the slow automation mechanisms of the GUI. Secondly, one has to take into account that the TAU is related to the measurement of ten averaged values. The variance and, therefore, the TAU is lower than when measuring without using Avasoft's internal averaging.

According to the calibration sheet of the spectrometer, the inaccuracy of the optical power is $u_{spec\_popt} = \pm 5\%$. After calculating the TAU and TBU, it turns out that $u_{A\_s\_popt}$ is two orders of magnitude smaller than $u_{B\_s\_popt}$ for all measurements. Therefore, the uncertainty in the average of the ten optical power measurements is determined by the formula VII-.6 $u_{R\_s\_popt} = \pm 5\%$.

6) Spectrometer measurement central wavelength uncertainty

The central wavelength (CWL) values are part of the same data set as the optical power values. That is, they are obtained in the same way. The TAU is calculated in the same way according to the equation VII-.1. The CWL uncertainty is calculated using the equation VII-.9, where the $FWHM$ value is obtained from the calibration protocol. For the spectrometer used, which has a grating of 500 lines/mm and a slit of 50 μm, the calibration protocol gives $FWHM = 5,5$ nm.

$$u_{spec\_cwl} = \frac{1}{2} \cdot FWHM = 2,75\ nm \qquad \text{(VII-.9)}$$

After calculating the TAU and TBU, it is again observed that $u_{A\_s\_cwl} <<< u_{B\_s\_cwl}$. Therefore, the uncertainty in the average of the ten measured CWL values is determined by the formula VII-.6 as $u_{R\_s\_cwl} = \pm 2.75$ nm.

7) Overview of uncertainties

For convenience, a summary of the measurement uncertainties is shown in the table VII-.1.

TABLE VII-.1. Overview of uncertainties.

Uncertainty description	uncertainty symbol	uncertainty value
LD temperature uncertainty	u_{R_TEC}	$\pm 0,1\ ^{\circ}$C
Photodetector horizontal uncertainty	$u_{R\_f\_hor}$	$\pm 0,005\%$
Photodetector vertical uncertainty	$u_{R\_f\_ver}$	$\pm 3,6\%$
Spectrometer CW mode LD current uncertainty	$u_{R\_s\_i\_cw}$	± 1 mA
Spectrometer PWM mode LD current uncertainty for PLT5 520B	$u_{R\_s\_imax\_pwm\_gr}$	$\pm 6,6$ mA
Spectrometer PWM mode LD current uncertainty for PLT5 450B	$u_{R\_s\_imax\_pwm\_bl}$	$\pm 4,6$ mA
Averaged optical power measurement uncertainty	$u_{R\_s\_popt}$	$\pm 5\%$
Averaged central wavelength uncertainty	$u_{R\_s\_cwl}$	$\pm 2,75$ nm

VIII. DISCUSSION AND LIMITATIONS

A major limitation of conducted experiments is the use of a relatively simple design of an electronic circuit that was manufactured by hand using THT (Through Hole Technology). Furthermore, to achieve high-frequency performance, an application of SMD parts and ceramic capacitors would be beneficial. From that point of view, there might be some limitations on the impact on the generality of observations, as the results are affected both by the LDs as well as the driving circuitry. Though there are limitations caused by the rather simple technology that is applied in the presented case, the obtained results for the power characteristic are in good correlation with the expectations given by the theory.

Three types of experiments were performed to test and subsequently characterize the selected LDs. The LDUTs were first measured in CW mode, which confirmed and extended their catalog parameters and characteristics.

Then followed PWM slow mode or pulse width modulation with a slow rising edge. It is the rising edge delay that enables PWM frequency control of the LUDT output, which is best seen in the ability to change the lasing threshold depending on the frequency of the control signal. In this mode, it was possible to change the threshold from **2.5 - 9.9%** PWM (I_{ld} = 216.1 mA) and **2 - 6.7%** PWM (I_{ld} = 148.1 mA), for frequencies between 10–50 kHz. Frequencies higher than the aforementioned range caused nonlinearities in the waveform, and lower frequencies lead to measurement error. As the frequency increases, the characteristics converge to the CW regime, and this is consequently associated with the increase in the impact of elevated temperature.

The third control method applied was the PWM fast mode, where the aim was to control the LDUT using as rectangular PWM signal as possible. An electrical circuit was constructed for this purpose and the following measurements confirmed linear waveforms, with minimal lasing threshold shift as well as the minimal effect of temperature on the threshold. The measurements were conducted again in the frequency range of 10–50 kHz, where the lasing threshold change was **0.06 - 0.195%** (I_{ld} = 216.1 mA) and **0.05 - 0.195%** (I_{ld} = 148.1 mA). Table VIII-.1 shows a summary of the most important experimental results obtained within the conducted research.

TABLE VIII-.1. Range of LD threshold possible frequency control 10–50 kHz .

LD	**PLT5 520B**	**PLT5 450B**
threshold W_{th} PWM **slow**	2.5 - 9.9%	2 - 6.7%
threshold W_{th} PWM **fast**	0.06 - 0.195%	0.05 - 0.195%

By redesigning the control circuit for LD switching, an increase in operating frequency was achieved. Compared to the PWM slow variant, which was based on the test function of a commercially available current driver, PWM fast characteristics are more linear. The aim was that the test frequency range would not be significantly influenced by the control electronics itself (see Fig A-B.1. and A-C.1.). Also, lower P_{opt} [W] levels were easier to achieve with PWM compared

to CW control, as it was not necessary to overcome the current threshold. As the effect of switching frequency was minimal for the PWM fast version, the temperature remains the primary factor to assess LD parameters. In conclusion, it can be therefore concluded that with proper LD control, optimal control can be achieved even with simple PWM modulation without the need for complex control with adjustable current sources.

IX. CONCLUSIONS

The presented paper shows how the PWM current drive changes the optical parameters of two specific commercially available LDs. Acquired results represent specifications beyond the readily available datasheet parameters that might be usable for researchers and engineers to apply these LDs in settings that require high-precision driving of the LD optical output achievable via the PWM method. Due to the increased interest in these performance characteristics of LDs among the scientific and engineering community, it might be worth considering for both LD and LD driver manufacturers to make these characteristics readily available to their prospective users. For those who might be interested in measuring these characteristics on their own, this paper also provides a methodology to follow.

Experiments demonstrated that with the chosen LDs, it is possible to fine-tune the output spectral bandwidth in the order of units of nanometers. For the follow-up experiments, it is, therefore, planned to measure coherence length with the use of an interferometer. Author considers another following experiment which will deal with the measurement of near- and far-field using the same modulation methods to investigate energy profile distribution. Other applications may include use for reflectometry (optical time domain reflectometry) or precise pulses telecommunication systems, or even medical applications.

.

APPENDIX A PEAK WAVELENGTH CHARACTERISTICS

A. CW

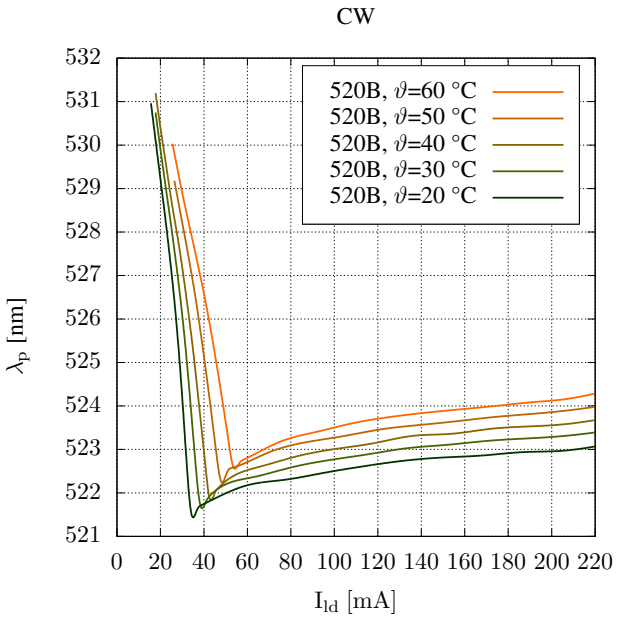

FIGURE A-A.1. PLT5 520B peak wavelength characteristics in CW mode.

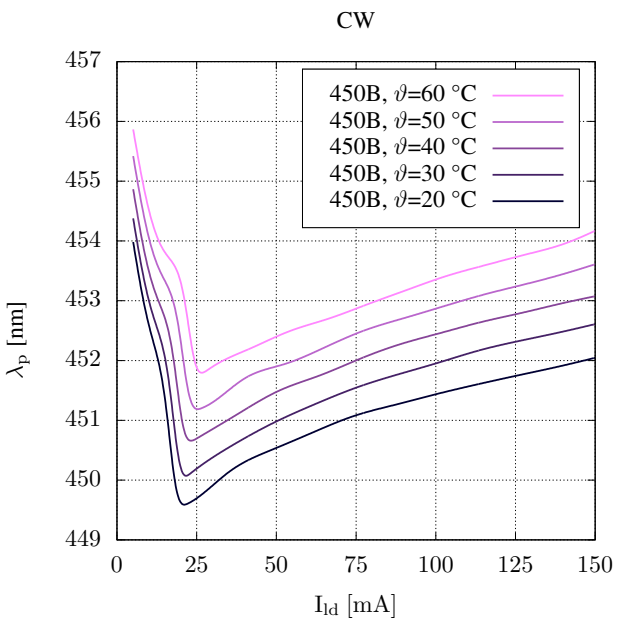

FIGURE A-A.2. PLT5 450B peak wavelength characteristics in CW mode.

B. PWM SLOW

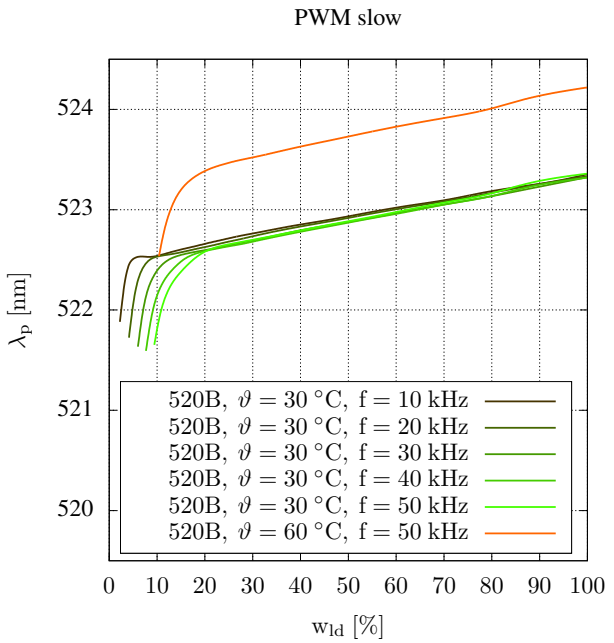

FIGURE A-B.1. PLT5 520B peak wavelength characteristics in PWM slow mode.

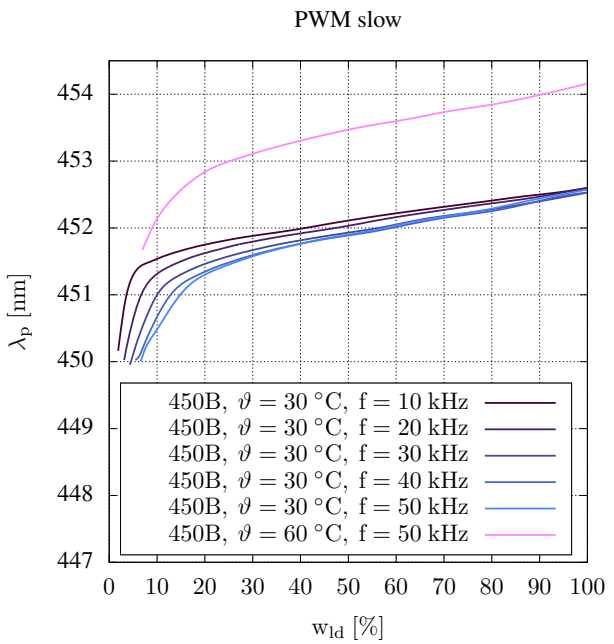

FIGURE A-B.2. PLT5 450B peak wavelength characteristics in PWM slow mode.

C. PWM FAST

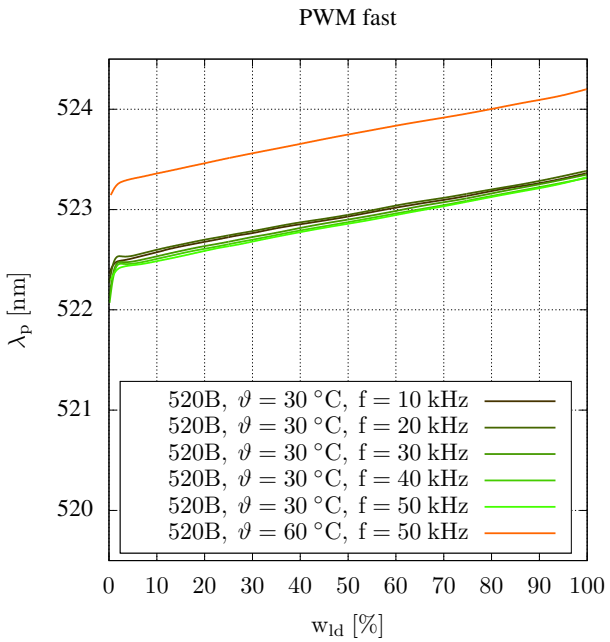

FIGURE A-C.1. PLT5 520B peak wavelength characteristics in PWM fast mode.

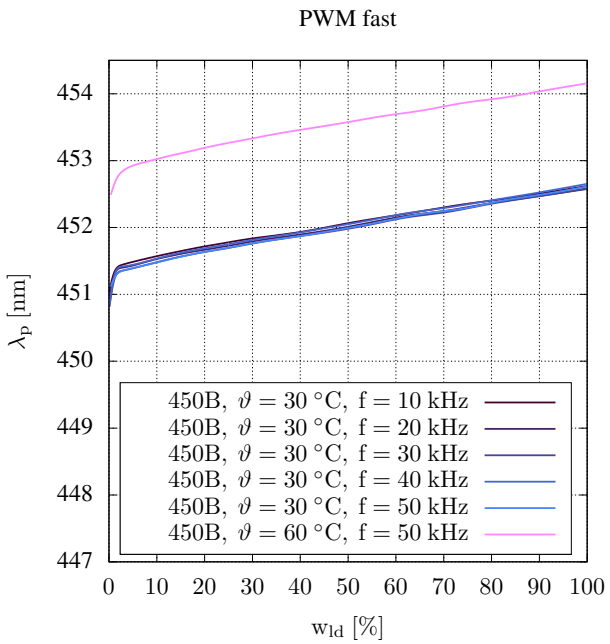

FIGURE A-C.2. PLT5 450B peak wavelength characteristics in PWM fast mode.

REFERENCES

[1] S. Ngcobo, I. Litvin, L. Burger, and A. Forbes, "A digital laser for on-demand laser modes," Nature Communications, vol. 4, no. 1, 2013.

[2] T. L. Paoli and J. E. Ripper, "Direct modulation of semiconductor lasers," Proceedings of the IEEE, vol. 58, no. 10, pp. 1457–1465, 1970.

[3] R. S. Tucker, "High-speed modulation of semiconductor lasers," IEEE Transactions on Electron Devices, vol. 32, no. 12, pp. 2572–2584, 1985.

[4] R. G. Hunsperger, "Direct modulation of semiconductor lasers," Advanced Texts in Physics, pp. 281–297, 2002.

[5] S. Inoue, "Laser Driving Apparatus - Panasonic Corporation," LASER DRIVING APPARATUS - PANASONIC CORPORATION, 26-Nov-2009. [Online]. Available: https://patentimages.storage.googleapis.com/dd/4b/6d/2be2628eb624d3/US20090290609A1.pdf. [Accessed: 06-Nov-2022].

[6] F. R. Pereira, L. R. Monte, F. R. Bassan, E. Mobilon, and J. C. de Oliveira, "Experimental analysis of system performance in an EDFA with pump driven in PWM mode," 2011 SBMO/IEEE MTT-S International Microwave and Optoelectronics Conference (IMOC 2011), 2011.

[7] W. Miao, J. Huang, H. Chen, Y. Wang, L. Wang, S. Ding, and Y. Gan, "Simulation and analysis of pulse driving circuit for Semiconductor Laser," IOP Conference Series: Earth and Environmental Science, vol. 632, no. 4, p. 042076, 2021.

[8] W. Putchana, A. Ratanavis, and P. Buranasiri, "A circuit design of Laser Pulse Generator," Journal of Physics: Conference Series, vol. 1719, no. 1, p. 012088, 2021.

[9] Q.-H. Tran, B. Nakarmi and Y. H.Won, "An Optical Pulse-Width Modulation Generator Using a Single-Mode Fabry-Pérot Laser Diode," Journal of the Optical Society of Korea, vol. 19, no. 3, pp. 255-259, 2015.

[10] X. Qu, S. C. Wong, and C. K. Tse, "Color control system for RGB led light sources using junction temperature measurement," IECON 2007 - 33rd Annual Conference of the IEEE Industrial Electronics Society, 2007.

[11] Xiaohui Qu, Siu-Chung Wong, and C. K. Tse, "Temperature measurement technique for stabilizing the light output of RGB LED lamps," IEEE Transactions on Instrumentation and Measurement, vol. 59, no. 3, pp. 661–670, 2010.

[12] F. Zhao, J. Chen, H. Wu, Y. Zeng, G. Dong, G. Yang, B. Shieh, and S. W. Ricky Lee, "Lifetime and failure analysis of LEDs driven by the constant-amplitude current with pulse width modulation," 2022 23rd International Conference on Electronic Packaging Technology (ICEPT), 2022.

[13] A. Jha, M. K. Shah, S. Jha, L. R. Cenkeramaddi and S. Royo, "Current Modulation Induced Stability in Laser Diode Under High Optical Feedback Strength," in IEEE Access, vol. 9, pp. 49537-49546, 2021.

[14] N. Sabyrov, A. Abilgaziyev, and M. H. Ali, "Enhancing interlayer bonding strength of FDM 3D printing technology by diode laser-assisted system," The International Journal of Advanced Manufacturing Technology, vol. 108, no. 1-2, pp. 603–611, 2020.

[15] J. Kim, S. Ji, Y.-S. Yun, and J.-S. Yeo, "A review: Melt Pool Analysis for selective laser melting with continuous wave and pulse width modulated lasers," Applied Science and Convergence Technology, vol. 27, no. 6, pp. 113–119, 2018.

[16] M. Berendt, H. Barbosa, J. Tomé, and M. Melo, "Laser diode pulse modulation in sensing and materials processing," Semiconductor Lasers and Laser Dynamics IX, 2020.

[17] A. Tariq, T. Islam, M. J. Javed, and M. H. Sayyad, "Design and characterization of a 3D-printer-based diode laser engraver," Second iiScience International Conference 2021: Recent Advances in Photonics and Physical Sciences, 2021.

[18] S. Vasanth and T. Muthuramalingam, "Development of laser beam machining using power diode laser for leather cutting application," Journal of Physics: Conference Series, vol. 1969, no. 1, p. 012024, 2021.

[19] A. Durna, J. Fries, L. Hrabovsky, A. Sliva, and J. Zarnovsky, "Research and development of laser engraving and material cutting machine from 3D printer," Management Systems in Production Engineering, vol. 28, no. 1, pp. 47–52, 2020.

[20] S. Vasanth, T. Muthuramalingam, S. Surya Prakash, S. Shriman Raghav and G. Logeshwaran, "Experimental investigation of PWM laser standoff distance control for power diode based LBM," Optics Laser Technology, vol. 158, Part A, 108916, 2023.

[21] J. Kinoshita, Y. Ikeda, Y. Takeda, M. Ueno, Y. Kawasaki, Y. Matsuba, and A. Heike, "Suppressed speckle contrast of blue light emission out of white lamp with phosphors excited by blue laser diodes for high-brightness lighting applications," Optical Review, vol. 19, no. 6, pp. 427–431, 2012.

[22] C. H. Lin, K. J. Pai, and P. H. Chen, "Development and implementation of a laser headlight system for electro-optic characteristic measurement and comparison," International Journal of Circuit Theory and Applications, vol. 48, no. 2, pp. 294–307, 2020.

[23] K.-J. Pai, C.-H. Lin, and P.-H. Chen, "Employing a laser headlight electrical system to measure and calculate electro-optic conversion efficiencies of blue-beam laser diodes," Electronics, vol. 9, no. 11, p. 1902, 2020.

[24] PLT5 520B Metal Can TO56. Datasheet OSRAM.
[25] PLT5 450B Metal Can TO56. Datasheet OSRAM.
[26] Thorlabs.com - Temperature Controlled Mount for Ø5.6 mm or Ø9 mm Laser Diodes.
[27] Operation Manual, Thorlabs Instrumentation, Laser Diode Combi Controller, ITC502 (-IEEE) ITC510 (-IEEE)
[28] TDS1000B and TDS2000B Series Digital Storage Oscilloscopes User Manual, ISBN: 071-1817-02
[29] User Guide, Thorlabs Instrumentation, PDA36A2 Si Switchable Gain Detector.
[30] Delta time accuracy: single shot, TDS1000B and TDS2000B Series Digital Storage Oscilloscopes User Manual, ISBN: 071-1817-02
[31] Operation Manual, Thorlabs Instrumentation, Laser Diode Combi Controller, ITC502 (-IEEE) ITC510 (-IEEE)

MIROSLAV SLOUKA received a B.Sc. (2019) and M.Sc. (2021) in the Field of Applied Electronics at VSB—Technical University of Ostrava, Faculty of Electrical Engineering and Computer Science, Department of Electronics. He is currently a Ph.D. student of Optoelectronics at the Department of Telecommunications at the same university. Miroslav worked for Siemens (2012) as an Electrical Test Engineer for asynchronous electric motors. Followed by the Development Center of HELLA (2015) as a Senior R&D Optics Lab Engineer and then Optics Design Engineer of automotive exterior lighting in the past. He is currently working in Astrum LT (2022) as Head of the Laser Systems Department.

LUKAS FOLTA was born in Olomouc, Czech Republic, in 1996. After a year of experience in repairing mobile phone motherboards and working as a service technician, he decided to expand his knowledge at the university in Brno. There he is currently studying his third year of a bachelor's degree in Microelectronics and Technology at the BUT - Brno University of Technology.

LADISLAV STANKE was born in Havířov, former Czechoslovakia in 1987. He received a bachelor's degree in optics and optoelectronics from the Palacky University Olomouc, Faculty of Science, Olomouc, in 2010, and master's degrees in digital and instrument optics and nanotechnology in 2012 and 2013, respectively. He was awarded his Ph.D. in applied physics at the same university in 2017. Later on, in 2021, he also received a master's degree in biomedical engineering at VSB—Technical University of Ostrava, Faculty of Electrical Engineering and Computer Science. Dr. Stanke is an interdisciplinary scientist with experience in academia as Laser Physicist and industry, where he focused mainly on optical engineering and lighting as a Lead Lighting Engineer in an automotive company. He is currently an employee of the University Hospital Olomouc, Czech National e-Health Center, where he is responsible for the technical aspects of various research projects, especially biomedical sensors, signal, and image analysis. He is also an employee of the Department of Psychology, Faculty of Arts, Palacky University Olomouc, where he is responsible for areas of psychophysics and psychophysiology. His main interest is vision science, and therefore, in 2019, he became a co-founder of the Human-Light Interaction laboratory located at the same institution.

JAN LATAL (S'16–M'12) was born in Prostejov, Czech Republic. In 2006 he was awarded his B.Sc. degree, and in 2008 M.Sc. degree at VSB—Technical University of Ostrava, Faculty of Electrical Engineering and Computer Science, Department of Telecommunications. He defended his Ph.D. thesis in 2015, and he works in the field of Optoelectronics, Wireless Optical Communications, Optical Communications and Distributed Temperature Sensing Systems.

He is a member of the Czech Light Society, SPIE, OPTICA (formerly OSA), and the Czech Photonics Society, as well as a member of the Institute of Electrical and Electronics Engineers (IEEE)

From 2010 to 2017, he was Editor-in-Chief of the journal Advances in Electrical and Electronic Engineering, and between years 2017 to August 2021, he was Associate Editor-in-Chief, and next from September 2021, he was back Editor-in-Chief position again on the editorial board. He was invited in 2019 to join the Editorial Board of the Optical and Quantum Electronics journal till now.

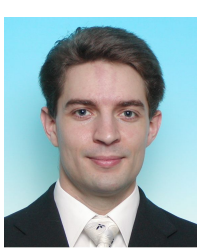

PETR SISKA was born in 1979 in Kromeriz. In 2005 he finished his M.Sc. study at the VSB–Technical University of Ostrava, Faculty of Electrical Engineering and Computer Science, Department of Electronic and Telecommunications. Three years later, he finished his Ph.D. study in Telecommunication technologies. In 2019 he became an Associate Professor at the Department of Telecommunications. In his career so far, he has successfully solved 6 national or international projects as the main researcher and more than 20 as a co-researcher or a member of the research team. He is mainly interested in Optical communications, Fiber optic-based sensors and Distributed Sensing systems.